



Solution-based fabrication of copper oxide thin film influence of cobalt doping on structural, morphological, electrical, and optical properties

Samed Çetinkaya^{*1} 

¹Mersin University, Department of Medical Services and Techniques, Türkiye, samedcetinkaya@mersin.edu.tr

Cite this study:

Çetinkaya, S. (2024). Solution-based fabrication of copper oxide thin film influence of cobalt doping on structural, morphological, electrical, and optical properties. Turkish Journal of Engineering, 8 (1), 107-115

Keywords

Chemical bath deposition
Copper
Cobalt
Doping
Activation energy

Research Article

DOI: 10.31127/tuje.1290655

Received:01.05.2023

Revised: 02.06.2023

Accepted:06.06.2023

Published:15.09.2023



Abstract

In this study, Cobalt (Co) doped Copper Oxide (CuO) films at different concentrations were deposited on glass substrates, using the Chemical Bath Deposition (CBD) method. The films were characterized by Field Emission Scanning Electron Microscopy (FESEM), X-Ray Diffraction (XRD), Ultra Violet-Visible Spectroscopy (UV-Vis.) and two-point contact method. The FESEM images showed that nanoplates formed increased in size and voids on the films surface decreased with increasing Co concentration. The XRD patterns revealed an increase in crystallite size with increasing (from 14.40 to 18.60 nm) Co concentration and no secondary phase was formed. The Energy-dispersive X-ray spectroscopy (EDS) spectra showed the presence of Co in the film composition with increasing concentration. The results of UV-Vis. spectroscopy showed that band gap values could be changed with Co doping and thus the CuO band gap could be adjusted with the Co doping. The temperature-dependent current-voltage measurement results obtained with the two-point contact method showed that activation energy levels increased (from 0.134 to 0.232 eV) with increasing Co concentration. It was also observed that the conductivity increased with increasing temperature.

1. Introduction

The decreasing fossil-based fuel reserves in the face of increasing energy demand has increased the interest in researching renewable alternative energy sources. Among the renewable energy sources, the most efficient and renewable energy source is solar energy [1]. Various materials have been developed to generate electricity from solar energy. Among them, nano-structured materials are widely used in this field due to their unique and interesting properties. These properties (such as electronic, magnetic, optical and structural properties) are characteristic of the nano-structured materials used and can be improved [2]. The surface properties of these structures affect their physical and chemical properties. For example, the photoconductivity properties of these structures vary depending on the surface area/volume ratio of the nanostructured material used and/or the porous structures on the surface. For this reason, these structures have been classified in the literature with various definitions such as nano-particles, nano-plates, nano-tubes, nano-rods, nano-flowers, and nano-spheres

[3]. Nano-structured materials with such different morphologies can be produced by doping various elements. Nanostructured materials are of great interest to researchers because they exhibit interesting properties in different applications as a result of the doping of transition metal oxides.

Among them, copper oxide (CuO) is an important transition metal oxide that exhibits p-type electrical conductivity and has a limited band gap and is a semiconductor with monoclinic crystal structure ($E_g=1.2-1.8$ eV) [4-6]. CuO is a nanotechnological material with gas sensors, biosensors, chemical sensors, solar cell absorber, high temperature (Tc) superconductors, lithium-ion batteries and catalysts applications [7]. In order for this material to be used in such a variety of fields, it must be produced in a cost-effective and environmentally friendly manner. Various deposition methods have been developed to fabricate for doped and undoped CuO nanostructures for instances; electrochemical deposition [8,9], physical vapor deposition [10,11], sol gel immersion [12,13] and sol-gel pin coating [14,15] deposition, radio frequency

sputtering deposition [16,17] and chemical bath deposition [17,18]. The chemical bath deposition method (CBD) offers many advantages for the production of thin films, including simplicity, proportional control of elements, cost-effectiveness, and deposition feasibility on large-area substrates. Many studies are being conducted to improve the performance of nanostructured materials such as CuO. In the literature, there are many studies conducted with the doping of different transition metals (such as Mn, Co and Fe) to improve the characteristics of semiconductors [19-21].

Transition metals (TMs) have high density, good conductivity and high melting-boiling temperatures [22-25]. Among these, Cobalt is preferred in studies due to its good effects on magnetic, hardness and electrical resistance [26,27]. CuO is an exciting semiconducting material with interesting structural and optical properties.

The effects of TMs-doping to the morphological, structural, and optical properties of the CuO films was reported in the literature.

In addition, The TMs- doped CuO thin films have attracted the attention of researchers for its applications in spintronic and ferromagnetism interactions [28,29].

According to the literature records we obtained as a result of our research, the effect of Co doping on the optical, structural, morphological and electrical properties of CuO films has not been studied yet by using the chemical bath deposition method.

In this study, it was aimed to determine the effect of Co doping concentration on the morphology, crystal structure, optical and electrical properties of CuO nano-structured films obtained by using chemical bath deposition method. Also, with this study, it is aimed to develop environmentally friendly materials and cost-effective methods for applications such as gas sensors, solar cells, catalysts, high temperature superconductors by improving the electrical and optical properties of CuO under the doping effect of cobalt ions.

2. Method

Doped and undoped CuO thin films were deposited using the CBD method on cleaned substrates following the established procedure [30]. Copper (II) Acetate Monohydrate ($\text{Cu}(\text{CH}_3\text{COO})_2 \cdot \text{H}_2\text{O}$) ($\geq 98\%$) (0.1 M) and Cobalt(II) Chloride Hexahydrate ($\text{CoCl}_2 \cdot 6\text{H}_2\text{O}$) ($\geq 98\%$) metal salts was used as starting solutions for Cu and Co, respectively. All chemicals used in the experiment were supplied by Merck KGaA. The films were deposited on standard microscope slides (7.5 cm * 2.5 cm). Chemical cleaning of the substrates has been completed by reference to previous studies as previous established procedure [20].

Copper (II) Acetate Monohydrate ($\text{Cu}(\text{CH}_3\text{COO})_2 \cdot \text{H}_2\text{O}$) ($\geq 98\%$) (0.1 M) was mixed with distilled water (double distilled water) as solvent in a 100 mL beaker to store pure CuO thin films. The solution was stirred to the obtain homogeneous solution at room temperature during 10 min.

Aqueous ammonia was added to the starting solution to adjust the pH (~ 10) of the solution. After the previously cleaned substrates were immersed in the bath

solution, the temperature of the solution was adjusted to $\sim 90^\circ\text{C}$.

($\text{Cu}(\text{OH})_2$) compound, which is formed by adding too much ammonia, turns into CuO with increasing temperature and starts to be stored on the substrate). After 20 minutes, the substrates removed from the solution were washed with double distilled water and left to dry at room conditions. This process was applied in the same way for the films to be deposited with cobalt added to the starting solution (atomic percent ratio (at. %) as 1, 3 and 5). Doped and undoped CuO thin films obtained after deposition were heat treated for 1 hour in an ash furnace (MKF106, Miprolab) at 573 K. According to the contribution ratio in the article, the samples are labelled as S0: undoped, S1: 1 at. %, S3: 3at. % and S5: 5at. % respectively.

Crystallographic structures of the films were investigated by X-Ray Diffraction (Rigaku Smartlab, X-Ray Diffractometer, Tokyo, Japan, X-ray diffraction device,) and $\text{Cu K}\alpha$ radiation in 0.01° steps ($\lambda = 1, 54059 \text{ \AA}$). The atomic ratios of the elements were determined using energy dispersion spectroscopy (EDS) (FEI EDS nova nano, NYSE, USA). The morphological and topological properties of the films were determined using Field emission scanning electron microscopy (FESEM, ZEISS EVO-LS10, NTS, Munich, Germany) The electrical properties of the samples were determined using a home-made Labview program-controlled voltage source computer interface with a precision multimeter (GW Instek, New Taipei, Taiwan) and a programmable power supply (GW Instek, New Taipei, Taiwan) using the two-point probe method with a temperature range of 300-500 K. Optical absorption spectra of pure and Co-doped CuO films were obtained using UV-Vis. Spectrophotometer (PerkinElmer) in the wavelength range of 200-1100 nm.

3. Results

The diffraction patterns of Co-doped and undoped CuO films as a result of X-ray diffraction spectrophotometer measurement are given in Figure 1. All the diffraction peaks match the monoclinic CuO (ICCD: 801916) phase, and no foreign peaks and/or a secondary phase were observed. It had been observed that these results are compatible with the literature. This can be interpreted as proof that Co doping penetrates into the CuO crystal lattice [30-32].

In Figure 1, it was seen that all films have the preferential orientation ($\bar{1}11$) and (111). Apart from these, (110), ($\bar{2}02$), (020), (202), ($\bar{1}13$), (022), (113), (311) and (004) peaks were also detected. In addition, it was observed that the ($\bar{1}11$) and (111) peak positions did not undergo a large shift in the peak positions with the contribution of Co. Table 1 clearly shows that the microstrain is directly proportional to the dislocation density and inversely proportional to the crystal size.

Dislocations are irregularities in a crystal that occur due to lattice mismatch from one part of the crystal to the other. These irregularities cause defects and strains in the crystal structure. Table 1 showed that the strains and strains in the crystal structure of the produced films were smaller compared to the undoped films. Also, D the

crystal size; ϵ , micro strain; ρ , defect density and d , distance between planes are calculated and given in Table 1. The positions of the peaks did not show a significant shift as the Co contribution had no or negligible effect on the strains in the lattice. Also, no extra peaks representing any copper-cobalt phase were detected, ultimately proving that this method can reliably produce samples in a single phase. In addition, since the ionic radii of Co^{+2} (0.74 Å) and Cu^{+2} (0.73 Å) are very close to each other, Co^{+2} can easily settle in the spaces left by the Cu^{+2} ion [30].

$$D = \frac{K\lambda}{\beta \cos \theta} \quad (1)$$

Here λ ; is the wavelength of X-ray radiation, K ; (fixed with a value of 0.94 not greater than 1) correction factor, θ ; is the Bragg diffraction angle and β ; is the width of the half-maximum of a vertex is the angular value of the vertices at full width [20].

Defective place density, which gives the number of defects in the structure, can be calculated with the following Equation 2 [20].

$$\delta = \frac{1}{D^2} \quad (2)$$

A low value of the defect location density indicates the presence of crystallized wells. The micro strain (ϵ) of the films can be calculated using Equation 3 [20].

$$\epsilon = \frac{\beta \cos \theta}{4} \quad (3)$$

Here; β is the full width half maximum and θ is the diffraction angle. The micro strain is caused by the ion diameter between the guest (Co, doping) element and the host (Cu, doped) element. However, since the ionic diameters of these two elements are very close to each other, it is thought that there is no significant change.

The crystallite size values listed in Table 2 increased from 14.40 nm to 18.60 nm with increasing Co doping. According to Table 1, the increase in cobalt concentration increases the crystallite dimensions. It is seen that the increase in the crystallite size causes a decrease in the band gap. It was found that the increase in cobalt concentration caused the formation of other phase peaks of monoclinic CuO. This increase in peak density can be attributed to the increase in the crystallinity of the films.

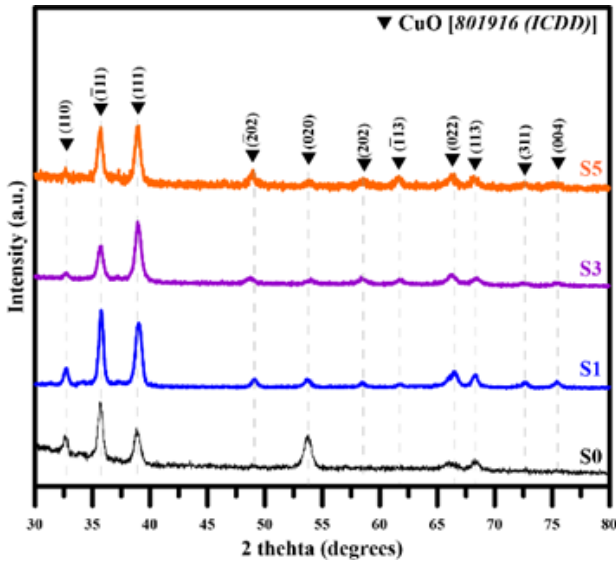


Figure 1. Diffraction patterns of Co-doped and undoped CuO films (S0: undoped, S (1-5): Co-doped CuO films).

The mean crystallite size (D) was calculated from the full width (β) of the half-maximum of a peak using the Scherrer formula, using Equation 1.

Table 1. Some structural parameters obtained and calculated from the films (D , crystal size; ϵ , micro strain; ρ , defect density; d , interplane spacing).

Samples	(111)		(111)		(020)		D (nm)	ϵ (10^{-4})	ρ (10^{15} cm^{-2})
	2θ ($^\circ$)	d (Å)	2θ ($^\circ$)	d (Å)	2θ ($^\circ$)	d (Å)			
S0	35,672	2,510	38,810	2,318	53,670	1,707	14,40	29,19	4,91
S1	35,735	2,511	39,000	2,308	53,770	1,704	16,00	23,28	4,22
S3	35,676	2,514	38,920	2,312	54,050	1,695	17,20	23,25	4,19
S5	35,669	2,515	38,875	2,315	53,870	1,700	18,60	23,09	4,14

Table 2. Variation of CuO:Co films on atomic doping ratio percentages, crystallite sizes and optical band gaps.

Samples	Atomic contribution ratio (%)	Crystallite Size (nm)	Forbidden energy gap (eV)
S0	0	14,40	1,64
S1	1	16,00	1,55
S3	3	17,20	1,52
S5	5	18,60	1,44

FESEM surface morphology images of Co-doped and undoped CuO films are given in Figure 2 and EDS spectrum is given in Figure 3. As can be seen in Figure 2, it was observed that the surface properties of CuO films changed significantly as a function of Co concentration. It was observed that the Co concentration had a significant effect on the shape and size of the nanostructures. It was found that the undoped CuO film has a regular and homogeneous distribution of micron-sized plates, on the

other hand, these plates increase in size (from ~200nm to ~800nm) with the increase of Co concentration, and agglomerated heaps are formed on the film surface. In addition, it was observed that the gaps between the nano-sized plates decreased with the increase in the amount of Co.

Here, it has been reported by researchers in the literature that the increase in grain size may have a positive contribution to the conductivity mechanism as it

will create less obstacle for the charge carriers [30,31]. Figure 3 shows the chemical composition analysis result using the EDS spectrum of Co-doped and undoped CuO films. In the EDS spectrum, it was observed that there are peaks of Cu, Co and O elements. In Figure 3, it is clearly

seen that the Co element enters the CuO matrix with the increase in the doping ratio. It can be interpreted by considering the obtained structural measurement (XRD) results that Co doping has a significant effect on the characteristic properties of CuO films.

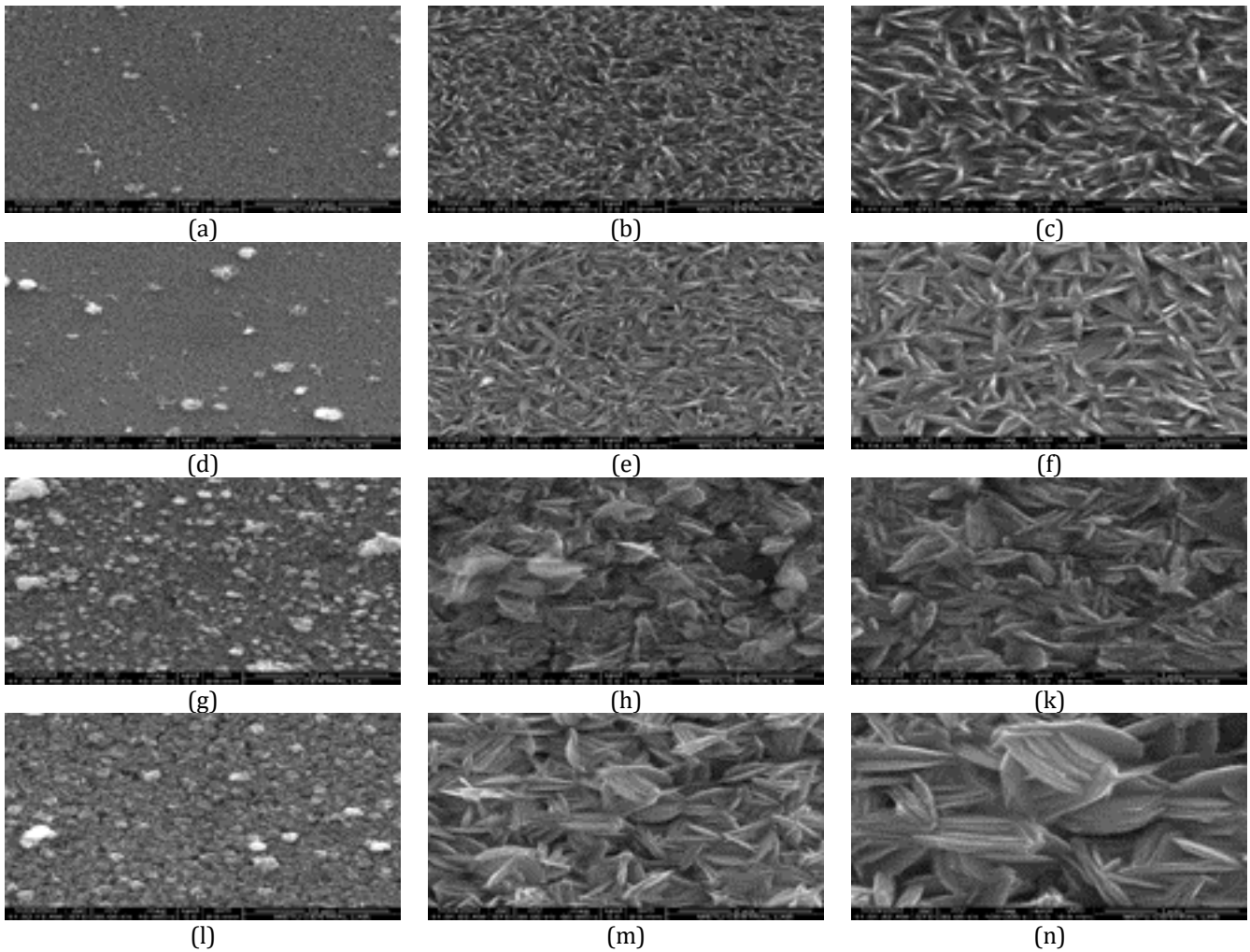


Figure 2. (a) 10kX, (b) 50kX and (c) 100kX, S0 coded samples; (d) 10kX, (e) 50kX and (f) 100kX belong to the S1 coded samples; FE-SEM surface morphology images of (g) 10kX, (h) 50kX and (k) 100kX and (l) 10kX, S3 coded samples, (m) 50kX and (n) 100kX, S5 coded samples.

The optical properties of the films were calculated using the absorption spectra collected by UV-Vis. spectrophotometer. Tauc plots of the allowed band gap of the films as a function of Co contribution are given in Figure 4. Equation 4 was used to obtain the band gap values.

$$ahv = C(hv - E_g)^m \quad (4)$$

where C is a constant, a is the optical absorption coefficient and $m = 1/2$ for direct allowed transition semiconductors. The point where the linear part of the Tauc plots shown in Figure 4 intersects the hv axis gives the band gap values of the films [33-35].

The calculated band gap of the forbidden energy of the films for S0-S5 at atomic concentrations of Co element, respectively; S0: 1.64, S1: 1.55, S3: 1.52, and S5: 1.44 eV. The results are consistent with the literature [20]. Moreover, the change in band gap values versus Co doping is shown in Figure 4. It is seen that the E_g values

of the films decrease with increasing Co concentration. This narrowing in the allowed band gap according to the additive concentration can be interpreted as a result of the band gap and crystallite size being inversely proportional to each other (Table 2). Similar behavior, Bayansal et al. [20] reported with the relationship they obtained as a result of cobalt doping. Bayansal et al. [20] reported this as the result of an effect that can be seen in nanoparticles due to the quantum confinement effect. Consequently, a change in particle and/or crystallite size directly affects the optical properties. As a result, Co doping has shown that it can be used to regulate the E_g of CuO films.

In order to find the electrical activation energies of the impurity levels, the conductivity-temperature characteristics of the samples were investigated in the 300-500 K temperature range by using the software prepared using LabVIEW graphical programming language and programmable precision multimeter (GW Instek 8261A) and voltage source (GW Instek 4303S) equipment. Conductive spring contact tips to be used in

two contact methods are used in FEIN brand and scientific circuit conductivity test (ICT) processes. These are gold-plated contact tips with a diameter of 0.6mm, low contact resistance, and stable measurement between -45° and +200°C. Contact tips can be made to contact the surface of the films directly or by taking an Ohmic contact. Here, ohmic contacts are formed on the surface of the films with silver conductive paste in order to increase the conductivity on the contact surface. Contributions from the contacts have been calibrated

and eliminated to be minimized by software. According to the solid state theory of semiconductors, the temperature dependence of the dark electrical resistance of a semiconductor with one or more impurity levels is given by Equation 5 [39].

$$R(T) = R_0 e^{\frac{E_g}{2kT}} + \sum_{(i=1)}^n R'_{0,i} e^{\frac{\Delta E_i}{kT}} \quad (5)$$

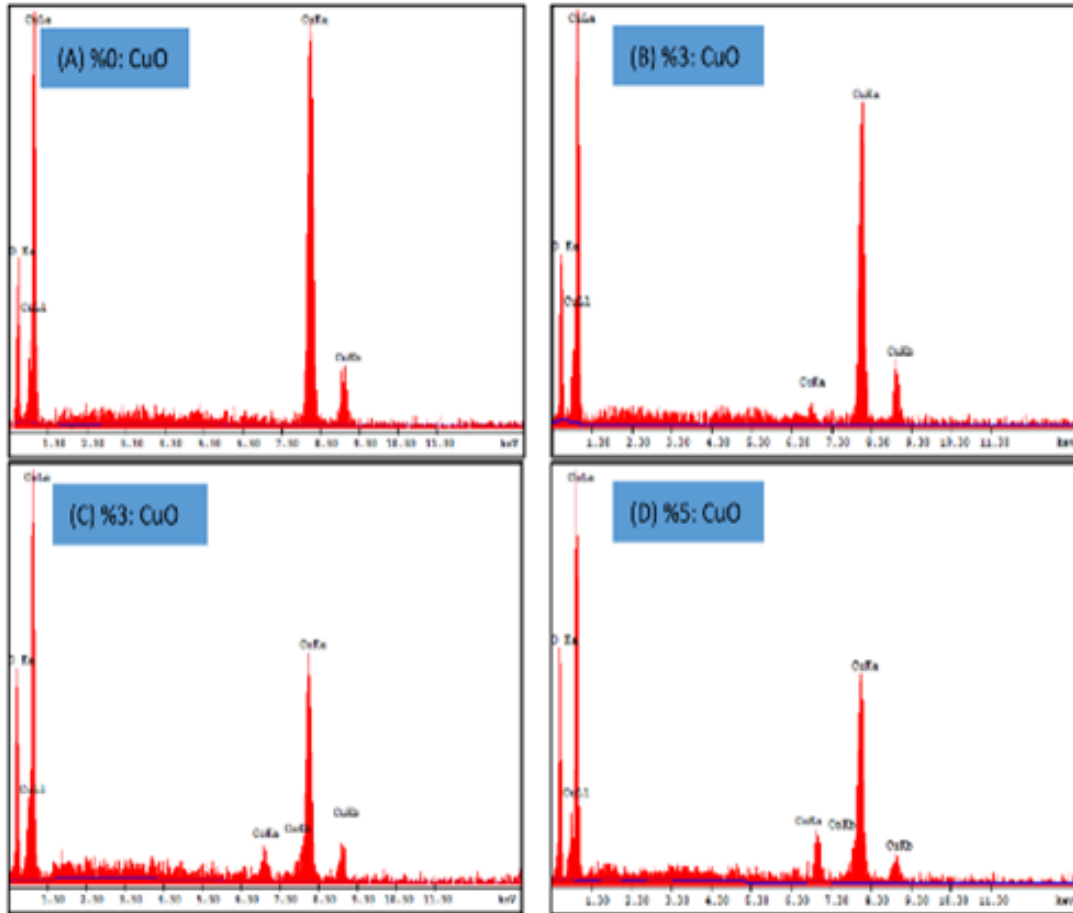


Figure 3. Energy dispersion X-ray spectroscopy (EDS) spectra of (a) S0, (b) S1, (c) S3 and (d) S5 coded samples.

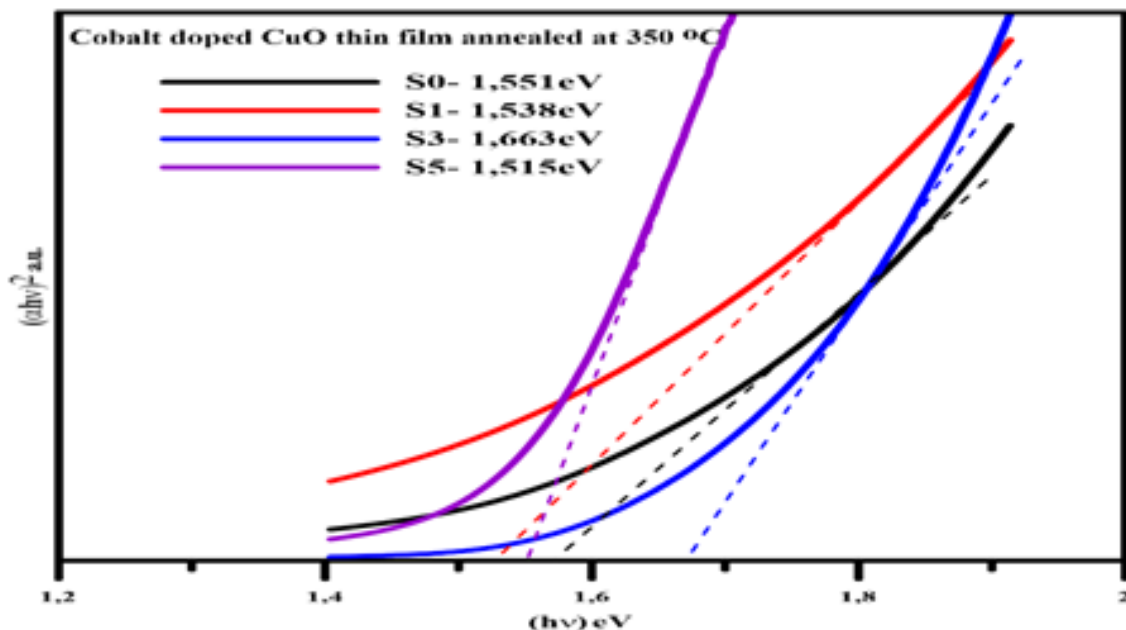


Figure 4. Direct-allowed bandgap energy values of Co-doped and undoped CuO thin films.

Here, the constants R_0 and $R_{(0,i)}$ define the temperature-dependent forbidden band gap energy, E_g the impurity level ionization energy, k the Boltzmann constant, and T the absolute temperature in Kelvin. In the temperature range region of 300-390 K, the overall electrical conductivity of a semiconductor is suppressed by the charge carriers produced by the ionization of impurity levels, and therefore the second term in Equation 5 dominates in this temperature range. With the increase towards high temperatures, the variation of the resistance of the semiconductor with temperature changes through band-to-band electronic transitions. Under these conditions, charge carriers acquire sufficient thermal energy to switch between bands [36]. According to the information above, they can be considered as independent values in the temperature ranges corresponding to the two terms appearing in Equation 5. Therefore, a series of linear trends appear, showing the band gap of the forbidden energy and a range of impurity levels (band gap states) in that gap. The slope of these linear regions formed, the electrical conductivity for a semiconductor such as CuO, is governed by the ionization of charge carriers at impurity levels in the investigated temperature range [37].

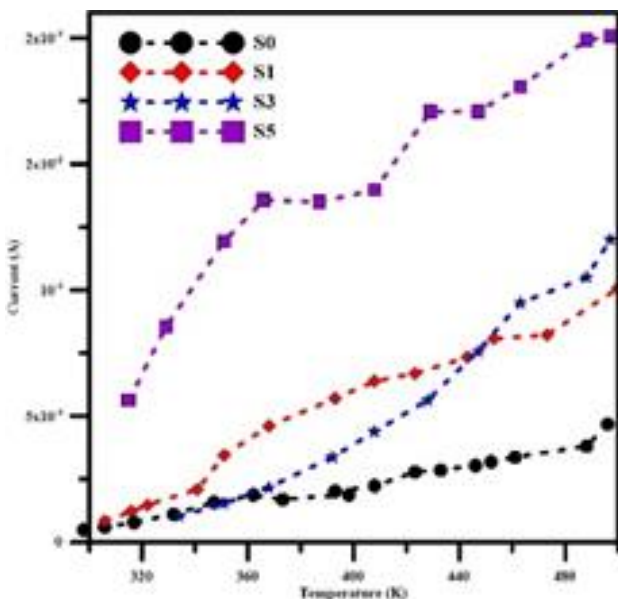
Therefore, the second term in Equation 5 is more dominant in R-T dependence. Upon increasing the temperature in the outer conductivity region, a decrease in electrical resistance (corresponding to a lower temperature range) is expressed by Equation 6 [36].

$$T = \sum_{(i=1)}^n R'_{(0,i)} \exp \left(\frac{\Delta E_i}{k R(T)} \right) \quad (6)$$

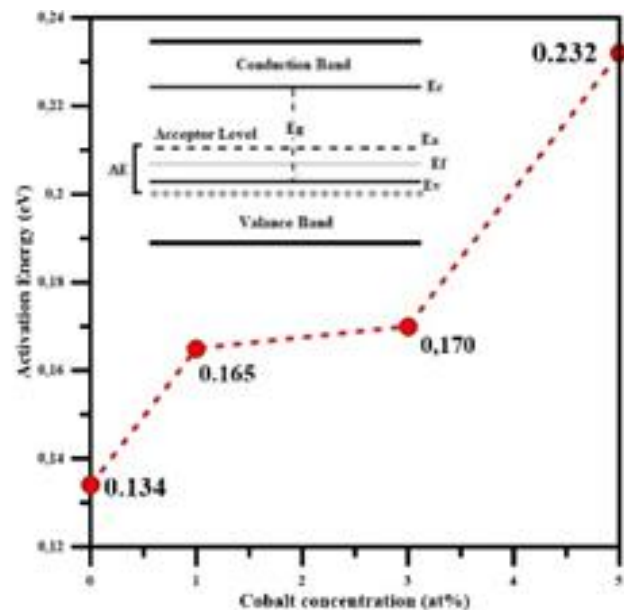
Only one linear region was detected in Co-doped and undoped CuO thin films, and an impurity level could be calculated for each sample. Using Equation 7, it can be written as [36];

$$\Delta E = k \frac{d(\ln R(T))}{d\left(\frac{1}{T}\right)} \quad (7)$$

Figure 5a shows the changes in the current depending on the temperature in the films (S0, S1, S3, and S5). By calculating the ionization energy values of the pollution (impurity) level against the Co additive concentration, S0: 0.134; S1: 0.165; S3: 0.17 and S5: 0.232 eV. Also, the change in activation energy values versus cobalt additive concentration is given in Figure 5b. The activation energy level represents the energy difference between the acceptor level and the valence band in the inner drawing shown in the graph in Figure 5b. Thus, the amount of energy required for the charge carriers located in these intermediate levels (pollution/impurity) between the valence and conductivity energy levels to pass into the conduction band and contribute to the electrical conductivity can be calculated using the temperature-dependent current voltage measurement technique. Thermally activated band conductivity is defined by Equation 6. Activation energy for thermally activated band conductivity; The majority depends on the charge carrier concentration and the impurity energy levels. The change in charge carrier concentration changes the Fermi energy level in the E_g energy range, resulting in an increase or decrease in the activation energy [38]. When the calculated forbidden energy band gap (E_g) values of the samples are examined, it is observed that the E_g values decrease (Figure 4) and the activation energy level values (Figure 5b) increase with the increase in the amount of doping. As Nguyen et al. reported in their study, this contradicts their interpretation of Donor-type load bearers. Because the CuO semiconductor used in our study has p-type electrical conductivity. For this reason, it can be interpreted that the increase in carrier concentration will decrease the Fermi energy level in the E_g energy range and this may cause an increase in the activation energy. Thus, it can be said that the results are compatible with the literature.



(a)



(b)

Figure 5. Variations of (a) current with temperature and (b) impurity levels with Co concentration.

According to the results obtained are compatible with the experimental results of XRD and FESEM analyzes (Figure 1 and Figure 2) because, according to these results, it is seen with the results of both methods that the crystallite and grain sizes increase with increasing Co concentration. As the crystallite size increases, the grain sizes increase, the contact surface areas between the grains increase, and therefore the gaps at the grain boundaries decrease. As a result, the scattering of carriers at grain boundaries is reduced [39]. As a result of this decrease, the number of load carriers participating in the transmission increases. Similar results were reported by Patil et al. [40]. The calculated activation energies are much smaller than the optical band gap energy ($\ll E_g/2$), which can be interpreted as the transmission of charge carriers from the valence band to the acceptor level [38].

4. Discussion

According to the results obtained valuable information given as below;

- ❖ According to X-ray diffraction spectrum data, it was determined that CuO and CuO:Co films have monoclinic crystal structure. It was determined that Co atoms penetrated CuO well and the preferential orientation of ($\bar{1}11$) and (111) did not change with the increase in Co doping concentration. The increase in cobalt concentration increases the crystallite size. It is seen that the increase in crystallite size causes an increase in the activation energy values depending on the thermal conductivity together with the band gap. The crystallite size of undoped CuO (14.40 nm) increased with doping and the highest crystal size was calculated as 18.60 nm for the film with the highest Co concentration (S5).
- ❖ According to the FESEM images, a structure consisting of dense void-free nano-sized plates was seen. It was observed that the surface morphologies of the films changed depending on the Co concentration. It was observed that the gaps between the nano-sized plates decreased with the increase in the amount of Co. It has been observed that the average dimensions of these structures vary between 200-800 nm. It has been interpreted that Cu and Co elements have different atomic radii (Co: 167 pm; Cu: 157 pm) and electronegativity (Co: 1.88; Cu: 1.90) and the free surface energy and thermodynamic equilibrium states have an effect on the growth of CuO crystals. It was observed that the peaks of Cu, Co and O elements were observed in the EDS spectrum, and the change in the spectrum with Co concentration was clearly seen.
- ❖ Examining the optical behavior, it was determined that Co-doping was dominant on E_g of CuO films. This situation is directly related to the surface morphologies of the films produced. Because a change in particle/crystallite size directly affects the optical properties. The calculated band gap of the films was calculated as S0: 1.64, S1: 1.55, S3: 1.52 and S5: 1.44 eV for S0-S5, respectively, according to the atomic concentrations of Co element.
- ❖ It has been determined that Co doping, which has a significant effect on its electrical properties, increases the activation energy values. Activation energy values, S0: 0.14; S1: 0.16; S3: 0.17 and S5: 0.23 eV. It was found that as a result of the formation of larger nano-sized plates with the increase of the additive amount, the gaps between these nanostructures decreased. Since these gaps act as scattering centers for charge carriers, the increase in conductivity value is directly related to the surface morphology.

5. Conclusion

In this study, CuO films doped with CuO and atomic additive ratio (1.0; 3.0; 5.0%at.) were deposited on glass substrates by using chemical bath deposition technique. The effects of Co concentration in CuO host on structural, morphological, optical and electrical properties were investigated in detail.

Thus, according to all data obtained from XRD, FESEM and Optical band measurement results, it was observed that each of the structural, morphological and optical parameters had significant effects on the electrical behavior of Cobalt doped CuO thin films. The research results show that some physical parameters of the CuO can be easily controller via doping Cobalt.

Conflicts of interest

The authors declare no conflicts of interest.

References

1. Mishra, A. K., & Pradhan, D. (2021). Hierarchical urchin-like cobalt-doped CuO for enhanced electrocatalytic oxygen evolution reaction. *ACS Applied Energy Materials*, 4(9), 9412-9419. <https://doi.org/10.1021/acsaem.1c01632>
2. Kerli, S., & Kavgacı, M. (2021). Bakır oksit ince filmlere bor katkısının metil mavisi üzerindeki fotokatalitik etkisinin araştırılması. *Journal of Boron*, 6(2), 283-289. <https://doi.org/10.30728/boron.797645>
3. Yetim, N. K., Aslan, N., Sarioğlu, A., Sarı, N., & Koç, M. M. (2020). Structural, electrochemical and optical properties of hydrothermally synthesized transition metal oxide (Co₃O₄, NiO, CuO) nanoflowers. *Journal of Materials Science: Materials in Electronics*, 31, 12238-12248. <https://doi.org/10.1007/s10854-020-03769-x>
4. Johan, M. R., Suan, M. S. M., Hawari, N. L., & Ching, H. A. (2011). Annealing effects on the properties of copper oxide thin films prepared by chemical deposition. *International Journal of Electrochemical Science*, 6(12), 6094-6104.
5. Bayansal, F., Şahin, O., & Çetinkara, H. A. (2020). Mechanical and structural properties of Li-doped CuO thin films deposited by the successive ionic layer adsorption and reaction method. *Thin Solid Films*, 697, 137839. <https://doi.org/10.1016/j.tsf.2020.137839>

6. Diachenko, O., Kováč Jr, J., Dobrozhan, O., Novák, P., Kováč, J., Skriniarova, J., & Opanasyuk, A. (2021). Structural and optical properties of CuO thin films synthesized using spray pyrolysis method. *Coatings*, 11(11), 1392. <https://doi.org/10.3390/coatings11111392>
7. Alzaid, M., Sajjad, M., Ali, K., Jamil, Y., Akbar, L., Sattar, A., Rizwan, A., Suhale, A., Ahmad, H., Nouman, C. M., Ghani, M. U., & Umair, A. (2020). Enhanced structural and optical properties of copper oxide for solar cell applications. *Journal of Ovonic Research Vol*, 16(6), 405-412.
8. Sadale, S. B., Patil, S. B., Teli, A. M., Masegi, H., & Noda, K. (2022). Effect of deposition potential and annealing on performance of electrodeposited copper oxide thin films for supercapacitor application. *Solid State Sciences*, 123, 106780. <https://doi.org/10.1016/j.solidstatesciences.2021.106780>
9. Dhanasekaran, V., Mahalingam, T., Chandramohan, R., Rhee, J. K., & Chu, J. P. (2012). Electrochemical deposition and characterization of cupric oxide thin films. *Thin Solid Films*, 520(21), 6608-6613. <https://doi.org/10.1016/j.tsf.2012.07.021>
10. Huang, M. L., Lu, S. G., Zhou, J. J., Luo, B. S., & Li, Y. H. (2022). Metallic coloration with Cu/CuO coating on polypropylene nonwoven fabric via a physical vapor deposition method and its multifunctional properties. *The Journal of The Textile Institute*, 113(7), 1345-1354. <https://doi.org/10.1080/00405000.2021.1928995>
11. Mahana, D., Mauraya, A. K., Pal, P., Singh, P., & Muthusamy, S. K. (2022). Comparative study on surface states and CO gas sensing characteristics of CuO thin films synthesised by vacuum evaporation and sputtering processes. *Materials Research Bulletin*, 145, 111567. <https://doi.org/10.1016/j.materresbull.2021.111567>
12. Musa, A. M. M., Farhad, S. F. U., Gafur, M. A., & Jamil, A. T. M. K. (2021). Effects of withdrawal speed on the structural, morphological, electrical, and optical properties of CuO thin films synthesized by dip-coating for CO₂ gas sensing. *AIP Advances*, 11, 115004. <https://doi.org/10.1063/5.0060471>
13. Salam, S., Jose, B., Raphael, R., & Anila, E. I. (2021, February). Synthesis and characterisation of copper oxide thin films by double dip method. In *IOP Conference Series: Materials Science and Engineering*, 1070(1), 012011. <https://doi.org/10.1088/1757-899X/1070/1/012011>
14. Kabir, M. H., Ibrahim, H., & Billah, M. M. (2021, February). Effect of stabilizer on sol ageing for CuO thin films synthesized by sol-gel spin coating technique. In *AIP Conference Proceedings*, 2324, 030007. <https://doi.org/10.1063/5.0037501>
15. Baturay, S., Candan, I., & Ozaydin, C. (2022). Structural, optical, and electrical characterizations of Cr-doped CuO thin films. *Journal of Materials Science: Materials in Electronics*, 33(9), 7275-7287. <https://doi.org/10.1007/s10854-022-07918-2>
16. Wu, J., Gao, Q., Wei, G., Xiu, J., Li, Z., & Liu, H. (2021). Optical properties and laser-induced breakdown spectroscopy analysis of Al-or Co-doped CuO thin films prepared on glass by radio-frequency magnetron sputtering. *Thin Solid Films*, 722, 138572. <https://doi.org/10.1016/j.tsf.2021.138572>
17. Patwary, M. A. M., Ohishi, M., Saito, K., Guo, Q., Yu, K. M., & Tanaka, T. (2021). Effect of Nitrogen Doping on Structural, Electrical, and Optical Properties of CuO Thin Films Synthesized by Radio Frequency Magnetron Sputtering for Photovoltaic Application. *ECS Journal of Solid State Science and Technology*, 10(6), 065019. <https://doi.org/10.1149/2162-8777/ac0a98>
18. Reyes-Vallejo, O., Escorcía-García, J., & Sebastian, P. J. (2022). Effect of complexing agent and deposition time on structural, morphological, optical and electrical properties of cuprous oxide thin films prepared by chemical bath deposition. *Materials Science in Semiconductor Processing*, 138, 106242. <https://doi.org/10.1016/j.mssp.2021.106242>
19. Babu, M. H., & Podder, J. (2021). Bond length controlling opto-structural properties of Mn doped CuO thin films: an experimental and theoretical study. *Materials Science in Semiconductor Processing*, 129, 105798. <https://doi.org/10.1016/j.mssp.2021.105798>
20. Bayansal, F., Taşköprü, T., Şahin, B., & Çetinkara, H. A. (2014). Effect of cobalt doping on nanostructured CuO thin films. *Metallurgical and Materials Transactions A*, 45, 3670-3674. <https://doi.org/10.1007/s11661-014-2306-1>
21. Chaudhary, M., Singh, M., Kumar, A., Gautam, Y. K., Malik, A. K., Kumar, Y., & Singh, B. P. (2021). Experimental investigation of Co and Fe-Doped CuO nanostructured electrode material for remarkable electrochemical performance. *Ceramics International*, 47(2), 2094-2106. <https://doi.org/10.1016/j.ceramint.2020.09.042>
22. Singh, P., Singh, R. K. & Kumar, R. (2021). Journey of ZnO quantum dots from undoped to rare-earth & transition metal-doped & their applications. *RSC Advance*, vol. 11, pp. 2512-2545. <https://doi.org/10.1039/D0RA08670C>
23. Qamar, M. A., Javed, M., Shahid, S., & Sher, M. (2022). Fabrication of g-C₃N₄/transition metal (Fe, Co, Ni, Mn and Cr)-doped ZnO ternary composites: Excellent visible light active photocatalysts for the degradation of organic pollutants from wastewater. *Materials Research Bulletin*, 147, 111630. <https://doi.org/10.1016/j.materresbull.2021.111630>
24. Wang, B., Iqbal, J., Shan, X., Huang, G., Fu, H., Yu, R., & Yu, D. (2009). Effects of Cr-doping on the photoluminescence and ferromagnetism at room temperature in ZnO nanomaterials prepared by soft chemistry route. *Materials Chemistry and Physics*, 113(1), 103-106. <https://doi.org/10.1016/j.matchemphys.2008.07.031>
25. Zhang, S. G., Wen, L., Li, J. L., Gao, F. L., Zhang, X. W., Li, L. H., & Li, G. Q. (2014). Plasmon-enhanced ultraviolet photoluminescence from highly ordered ZnO

- nanorods/graphene hybrid structure decorated with Au nanospheres. *Journal of Physics D: Applied Physics*, 47(49), 495103. <https://doi.org/10.1088/0022-3727/47/49/495103>
26. Vinoth, S., Arulanantham, A. M. S., Saravanakumar, S., Rimal Isaac, R. S., Soundaram, N., Chidhambaram, N., ... & AlFaify, S. (2021). Enriched optoelectronic properties of cobalt-doped ZnO thin films for photodetector applications. *Journal of Materials Science: Materials in Electronics*, 32, 27060-27072. <https://doi.org/10.1007/s10854-021-07077-w>
 27. Babu, M. M. H., Podder, J., Tofa, R. R., & Ali, L. (2021). Effect of Co doping in tailoring the crystallite size, surface morphology and optical band gap of CuO thin films prepared via thermal spray pyrolysis. *Surfaces and Interfaces*, 25, 101269. <https://doi.org/10.1016/j.surfin.2021.101269>
 28. Bahoosh, S. G., Apostolov, A. T., Apostolova, I. N., & Wesselinowa, J. M. (2012). Theory of phonon properties in doped and undoped CuO nanoparticles. *Physics Letters A*, 376(33), 2252-2255. <https://doi.org/10.1016/j.physleta.2012.05.042>
 29. Babu, M. H., Podder, J., Dev, B. C., & Sharmin, M. (2020). p to n-type transition with wide blue shift optical band gap of spray synthesized Cd doped CuO thin films for optoelectronic device applications. *Surfaces and interfaces*, 19, 100459. <https://doi.org/10.1016/j.surfin.2020.100459>
 30. Yuksel, M., Pennings, J. R., Bayansal, F., & Yeow, J. T. (2020). Effect of B-doping on the morphological, structural and optical properties of SILAR deposited CuO films. *Physica B: Condensed Matter*, 599, 412578.
 31. Marotti, R. E., Giorgi, P., Machado, G., & Dalchiele, E. A. (2006). Crystallite size dependence of band gap energy for electrodeposited ZnO grown at different temperatures. *Solar Energy Materials and Solar Cells*, 90(15), 2356-2361. <https://doi.org/10.1016/j.solmat.2006.03.008>
 32. Oh, J., Ryu, H., & Lee, W. J. (2019). Effects of Fe doping on the photoelectrochemical properties of CuO photoelectrodes. *Composites Part B: Engineering*, 163, 59-66. <https://doi.org/10.1016/j.compositesb.2018.11.041>
 33. Du, Y., Gao, X., & Meng, X. (2019). Preparation and characterization of single-phased n-type CuO film by DC magnetron sputtering. *Physica B: Condensed Matter*, 560, 37-40. <https://doi.org/10.1016/j.physb.2019.02.037>
 34. Thi, T. V., Rai, A. K., Gim, J., & Kim, J. (2014). Potassium-doped copper oxide nanoparticles synthesized by a solvothermal method as an anode material for high-performance lithium ion secondary battery. *Applied surface science*, 305, 617-625. <https://doi.org/10.1016/j.apsusc.2014.03.144>
 35. Tauc, J., & Mentel, A. (1972). States in the gap. *Journal of non-crystalline solids*, 8, 569-585. [https://doi.org/10.1016/0022-3093\(72\)90194-9](https://doi.org/10.1016/0022-3093(72)90194-9)
 36. Erat, S., Braun, A., Çetinkaya, S., Yildirimcan, S., Kasapoğlu, A. E., Gür, E., ... & Ocakoglu, K. (2021). Solution-Processable Growth and Characterization of Dandelion-like ZnO: B Microflower Structures. *Crystals*, 12(1), 11. <https://doi.org/10.3390/cryst12010011>
 37. Bayansal, F., Çetinkara, H. A., Kahraman, S., Çakmak, H. M., & Güder, H. S. (2012). Nano-structured CuO films prepared by simple solution methods: plate-like, needle-like and network-like architectures. *Ceramics International*, 38(3), 1859-1866. <https://doi.org/10.1016/j.ceramint.2011.10.011>
 38. Nguyen T. T. H., Qui, T. L., Xuan, N. D., Hanh, N., Chinh, D. H. & Lin, V. D. (2005). Preparation and Characterization of Cobalt Doped ZnO Films. *Proceedings of The Eighth German-Vietnamse Seminar on Physics and Engineering*, Erlangen, April 3-8, 2005.
 39. Lee, J. H., Ko, K. H., & Park, B. O. (2003). Electrical and optical properties of ZnO transparent conducting films by the sol-gel method. *Journal of crystal growth*, 247(1-2), 119-125. [https://doi.org/10.1016/S0022-0248\(02\)01907-3](https://doi.org/10.1016/S0022-0248(02)01907-3)
 40. Jundale, D., Pawar, S., Chougule, M., Godse, P., Patil, S., Raut, B., ... & Patil, V. (2011). Nanocrystalline CuO thin films for H₂S monitoring: microstructural and optoelectronic characterization. *Journal of Sensor Technology*, 1(2), 34-36. <https://doi.org/10.4236/jst.2011.12006>



© Author(s) 2024. This work is distributed under <https://creativecommons.org/licenses/by-sa/4.0/>